SEMARAK ILMU PUBLISHING

Journal of Advanced Research in Fluid Mechanics and Thermal Sciences

Journal homepage:
https://semarakilmu.com.my/journals/index.php/fluid_mechanics_thermal_sciences/index
ISSN: 2289-7879

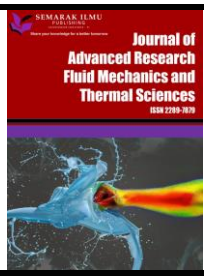

Investigation of the Thermal Performance of a Nanofluid-filled Grooved Cylindrical Heat Pipe for Electronics Cooling

Imène Saad[1], Samah Maalej[1], Mohamed Chaker Zaghdoudi[1,*]

[1] Laboratoire Matériaux, Mesures et Applications (MMA, LR11ES25), Institut National des Sciences Appliquées et de Technologie (INSAT), University of Carthage, Centre Urbain Nord, BP N° 676 – 1080 Tunis Cédex, Tunisia

ARTICLE INFO

Article history:
Received 5 April 2022
Received in revised form 12 August 2022
Accepted 20 August 2022
Available online 17 September 2022

Keywords:
Capillary grooves; electronics cooling; heat pipe; nanofluids; modeling

ABSTRACT

Thermal management of electric and electronic components is a critical issue and needs to consider enhanced cooling systems such as heat pipes. This study deals with the theoretical modeling of a nanofluid-filled copper cylindrical heat pipe for electronics cooling applications. The heat pipe includes helicoidal and trapezoidal capillary grooves. The model can predict the capillary limit as well as the heat transfer in the different sections of the heat pipe. The thermal resistances of the evaporation and condensation sections are calculated based on correlations for heat transfer, which are determined from experiments. Two working nanofluids are considered: water/CuO and water/Al_2O_3. The thermal performances are predicted for different concentrations and heat sink temperatures, and the heat pipe is positioned horizontally. For both nanofluids, the results indicate that augmenting the concentration of the nanoparticles leads to a capillary limit increase reaching up to 14 % and 25 % for water/Al_2O_3 and water/CuO, respectively, and an overall thermal resistance decrease reaching up to 51 % and 68 % for water/Al_2O_3 and water/CuO. Moreover, decreases up to 24 %, and up to 18 % in the evaporator wall temperatures are obtained for water/CuO and water/Al_2O_3 nanofluids, respectively. The nanofluid water/CuO gives the best thermal performance whatever the nanoparticle concentration and heat sink temperature.

1. Introduction

Two-phase cooling systems are efficient cooling devices that allow the transfer of high heat fluxes. Hence, they are one of the most promising technologies for the thermal control of electronic components since they have high carrying heat capacity and they can reduce temperature gradients and eliminate hot spots [1-3]. The enhancement of the heat exchange in two-phase cooling systems requires the improvement of the heat transfer by evaporation and condensation. Improvements in capillary structures are already widely explored. Therefore, new ways of optimizing two-phase cooling systems must be studied. Some of them propose using active techniques such as electrohydrodynamic effects, and other studies consider using new fluids [4,6]. Hence, during the last

* *Corresponding author.*
E-mail address: chaker.zaghdoudi@insat.rnu.tn

https://doi.org/10.37934/arfmts.99.2.135154

decay, the works have been oriented toward the exploration of the use of nanofluids in two-phase cooling systems.

The nanofluids are dispersions of nanoparticles in a base fluid. One of the main parameters to be considered to evaluate the potential of heat transfer is thermal conductivity. Indeed, the most widely used fluids, such as water, have a low thermal conductivity when compared to that solids. Inserting high conductive nanoparticles into a base fluid increases the effective thermal conductivity of the mixture. However, nanofluids present drawbacks for some applications. Indeed, the presence of nanoparticles decreases the heat capacity and increases the viscosity, which does not necessarily make the use of these fluids advantageous in single-phase forced convection applications. On the contrary, these drawbacks are much less influenceable in two-phase applications, for which the mass flow rates are generally low and heat exchanges are carried out mostly by latent heat.

In this study, the use of nanofluids in heat pipes is explored. A theoretical model is developed to determine the effects of the use of nanofluids on the capillary limit and the thermal performances of a cylindrical helicoidally grooved copper heat pipe. The combined effects of the nanoparticle concentration and the heat sink temperature are particularly highlighted.

2. Literature Survey on Studies Dealing with the Use of Nanofluids in Cylindrical Grooved Heat Pipes

Several research teams have studied the behavior of nanofluids in two-phase heat transfer devices such as heat pipes, thermosyphons, and loop heat pipes. This research area is still in the prototyping phase, to better understand the phenomena involved and the impact of the use of nanoparticles on various parameters, especially on wettability and latent heat. Table 1 presents a classification of experimental works dealing with cylindrical grooved heat pipes. The contribution of nanofluids to these systems remains a debate in the scientific community. Indeed, some works emphasize improvements in thermal performance while others report a deterioration of the heat transfer in such systems.

The nanofluids which have been tested consist of nanoparticles of pure metals such as silver, and copper [7-9,17,18,27]. Nanoparticles of metal oxides such as copper oxide (CuO), aluminum oxide (Al_2O_3), titanium oxide (TiO_2) and silicon oxide (SiO) are considered [10,11,13-21,23]. Other nanoparticles have been considered among them we distinguish carbon nanotubes (CNT), and graphene [12,22,24,31]. Some studies have considered hybrid mixtures of nanoparticles combining pure metals such as silver, copper, or iron with a metal oxide such as CuO or Al_2O_3 [17,29,30]. Water was selected as the base fluid in most studies. Some studies have considered alcohol or refrigerants as base fluids [13,28].

From this review, the main following conclusions can be drawn

i. Some studies reported an increase in the capillary limit that reaches up to 60 % [18,30]. The majority of these studies reported also a decrease in the heat pipe thermal resistance ranging between 1 % and 80 %. However, two studies reported an increase in thermal resistance [17,29]. Moreover, the majority of the study found that the evaporator temperature decreases in the range of 1 °C to 37 °C, except the work of Veerasamy *et al.,* [31] on graphene-water nanofluid who reported an evaporation temperature increase reaching up to 2 % when compared to that obtained with water-filled heat pipe.
ii. The heat transfer is enhanced by considering grooved capillary. However, the optimization of the groove the size and geometry of grooves should be accomplished by further experiments and theoretical simulations.

iii. The stability of the nanofluids and the nanoparticle concentration are critical parameters. The nanofluid stability is ensured by reducing the nanoparticle size and considering the appropriate surfactant.
iv. The heat pipe inclination significantly affects the thermal performance of the nanofluid-filled heat pipes. The optimum inclination depends on the heat pipe size and the working fluid.
v. The use of hybrid nanofluids in heat pipes is not much effective as pure nanoparticle-based nanofluids because hybrid nanofluids have high viscosity.

This work presents an efficient calculation tool to predict the thermal performance of a grooved heat pipe filled with nanofluids. The heat transfer coefficients in the evaporation and condensation sections, which are fundamental parameters in the thermal performance prediction, are determined by considering experimental results from the literature that are assessed to propose correlations based on the dimensionless analysis. The combined effects of the nanoparticle concentration and heat sink temperature are highlighted, which constitutes the novelty of this work.

3. Description of the Modeled Heat Pipe

The heat pipe is a sealed system that functions thanks to the capillary pumping principle (Figure 1). It is filled with a working fluid, commonly water, and its inner surface is lined with a wick structure, which enables the capillary pumping. As heat is dissipated from the heat source (electronic component) to the heat pipe wall, the working fluid is vaporized, and the vapor travels to the cooler region of the heat pipe where it condenses by releasing the latent heat of vaporization. The capillary wick then removes the condensate back to the evaporator section. This closed-loop circulation continues as long as heat is applied.

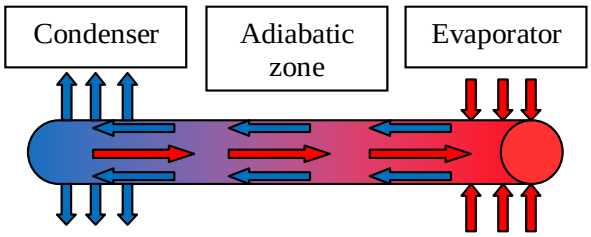

Fig. 1. Heat pipe operation principle

In this study, the heat pipe shape is cylindrical with 90 mm in length, and it is made of copper. Lengths of the evaporator, adiabatic, and condenser zones are 60 mm, 70 mm, and 60 mm, respectively. The capillary structure is composed of 75 helicoidally and trapezoidal grooves whose geometrical characteristics are detailed in Figure 2 and their values are given in Table 2.

Table 1
Literature survey on experimental studies on nanofluid-filled grooved cylindrical heat pipes

Date	Author	Overall dimensions (Diameter –Length) (in mm)	Groove dimensions (Width-Depth) (in mm)	Number of grooves	Nanofluid	Concentration (%)	Nanoparticle diameter (in nm)	Effects on the capillary limit	Effects on thermal resistance	Effects on the evaporator temperature
2005	Park *et al.,* [7]	6 – 300	nc	nc	Ag-H_2O	0.4 (vol)	nc	not studied	decrease	not studied
2005	Wei *et al.,* [8]	6 – 200	nc	nc	Ag–H_2O	5-10-15 ppm	10	not studied	-30 to -70 %	not studied
2006	Kang *et al.,* [9]	6 – 200	0.211 - 0.217	nc	Ag-H_2O	1 – 50 ppm	10 - 35	not studied	-50 % (10 nm) -80 % (35 nm)	not studied
2008	Naphon *et al.,* [10]	15 – 600	nc	nc	TiO_2-H_2O TiO_2- Alcohol	0.01 - 0.05 - 0.1 - 0.5 - 1.0 (vol)	21	not studied	not studied	not studied
2008	Yang *et al.,* [11]	8 – 350	0.25 - 0.2	nc	CuO-H_2O	0.5 - 2.0 (wt)	50	not studied	-15 to -39 %	from -1 °C to -13 °C
2009	Liu and Lu [12]	8 – 350	0.25 - 0.2	60	CNT-H_2O	1.0 to 2.5 (wt)	15	+25 %	-20 %	from -0.5 °C to -6°C
2009	Naphon *et al.,* [13]	15 – 600	nc	nc	TiO_2 -R11	0.01- 0.05 - 0.1 -0.5 - 1.0 vol%	21	not studied	not studied	not studied
2010	Liu *et al.,* [14]	8 – 350	0.20 - 0.25	nc	CuO-H_2O	0.5 - 2.0 (wt)	50	+35 %	-33 %	decreased
2010	Teng *et al.,* [15]	8 – 600	nc	nc	Al_2O_3-H_2O	0.5 - 1.0 - 3.0 (wt)	20 and 30	not studied	not studied	not studied
2010	Wang *et al.,* [16]	8 – 350	0.16-0.20-0.14*	70	CuO-H_2O	0.5 - 2.0 (wt)	50	+27-40 %	-50 %	from -1°C to -9°C
2011	Han and Rhi [17]	12 - 500	1.0 – 1.0	12	Ag-H_2O Al_2O_3-H_2O Ag/Al_2O_3-H_2O	0.005-0.05-0.1 vol%	27 (Ag) 89 (Al_2O_3)	not studied	+40 to +50%	not studied
2011	Liu *et al.,* [18]	8 - 350	0.16-0.20-0.14*	70	Cu-H_2O CuO-H_2O SiO-H_2O	0.063 - 0.25 (wt) 0.11 - 0.44 (wt) 0-2 (wt)	20 and 40 20 and 50 30	+60 % (Cu-40nm) +16 % (CuO-50nm) Not studied	-60 % (Cu – 40 nm)	not studied
2015	Ghanbarpour and Khodabandeh [19]	6.35-250	0.17-0.21*	nc	Al_2O_3 -H_2O TiO_2-H_2O	1-2.4 vol%	235 nm 120	not studied	not studied	not studied
2015	Yousefi and Heidari [20]	6-220	0.14-0.22	nc	Al_2O_3-H_2O	0.5 wt%	15	not studied	-23 to -31%	-2°C to -37 °C
2016	Aly *et al.,* [21]	15.87 - 550	nc-0.3	nc	Al_2O_3-H_2O	3.0 vol%	20	not studied	-18.2 %	from -1°C to -9°C
2016	Mehrali *et al.,* [22]	10 - 300	0.25 – 0.3	75	Graphene-H_2O	0.01 – 0.02 – 0.04 – 0.06 (wt)	nc	not studied	-60 %	from -0.2 °C to -10°C
2018	Thosre *et al.,* [23]	13 - 850	nc	nc	Al_2O_3-H_2O	0.05-0.10-0.15 vol%	nc	not studied	not studied	not studied
2018	Zhao *et al.,* [24]	(8-14) **-1600	nc	nc	Graphene-H_2O	0.01- 0.025-0.05-0.075 (wt)	0.8-1.2	not studied	not studied	not studied
2019	Gupta *et al.,* [25]	18 - 350	nc	nc	CeO_2-H_2O	0.5-1-1.5 vol%	40-60	not studied	decreased	not studied
2019	Sözen *et al.,* [26]	13 - 1000	nc	nc	$(Na,K,Ca)_{2-3}Al_3(Al,Si)_2Si_{13}O_{36}\cdot 12H_2O$ -H_2O	2 (wt)	nc	not studied	-9.63% - to -26.31 %	not studied
2019	Zhou *et al.,* [27]	1.9 - 130	0.17 - 0.22	12	Cu-H_2O	0.5 to 1.5 (wt)	nc	not studied	-54.5%	not studied
2020	Aydın *et al.,* [28]	15 - 400	nc	nc	$CaMg(CO_3)_2$/ $C_6H_6O_2$	2 (wt)	nc	not studied	-17% to -22%	not studied
2020	Martin *et al.,* [29]	15-1000	nc	nc	Fe+CuO-H_2O	2 (wt)	30-40/38	not studied	+16.91 %	decreased
2020	Pandya *et al.,* [30]	10.5-1000	0.79 - 1.3	28	CeO_2+MWCNT - H_2O	0.25 - 1.75 vol%	nc	+61.27%	-30%	not studied
2020	Veerasamy *et al.,* [31]	9.5-200	nc	nc	Graphene-H_2O	0.6, 0.75 vol%	150-200	not studied	-1.1% to -53.1%	+2%

* Trapezoidal grooves: height-bottom width-top width, ** 8 for the evaporation section and 14 for the condenser, (vol): volume concentration, (wt): weight concentration

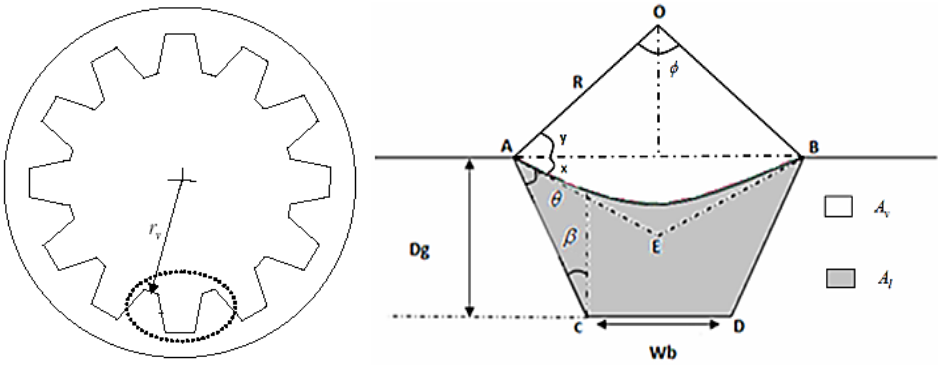

Fig. 2. Geometrical characteristics of the grooves

Table 2
Geometrical characteristics of the heat pipe

Parameters	Values
Heat pipe length, L_t	190 mm
Evaporator length, L_e	60 mm
Condenser length, L_c	60 mm
Outer diameter, D_o	15.87 mm
Wall thickness, t_w	0.58 mm
Number of grooves, N_g	75
Groove height, D_g	0.3 mm
Groove width at the bottom of the groove, W_{gb}	0.266 mm
Groove width at the top of the groove, W_{gt}	0.599 mm
Angle between the groove and the heat pipe axis, α	20 °
Angle β	29

4. Modeling of the Capillary Limit and Heat Transfer

4.1 Modeling of the Capillary Limit

A heat pipe operates properly when the capillary pumping, ΔP_c, is efficient to compensate for the pressure losses in the liquid and vapor phases, ΔP_l and ΔP_v, as well as the hydrostatic pressure, ΔP_g, according to

$$\Delta P_c \geq \Delta P_l + \Delta P_v + \Delta P_g \tag{1}$$

The driving capillary pressure can be expressed by

$$\Delta P_c = 2\,\sigma\cos(\theta)\left(\frac{1}{r_{ce}} - \frac{1}{r_{cc}}\right) \tag{2}$$

σ is the surface tension and θ is the contact angle. r_{ce} and r_{cc} are the minimum and the maximum capillary radii in the evaporator and condenser sections, respectively (Figure 2). They are given by the following expressions (Appendice 1)

$$r_{ce} = \frac{D_g}{1+sin(\beta+\theta)} \tag{3}$$

$$r_{cc} = \frac{D_g\,tan(\beta)+0.5\,W_{gb}}{cos(\beta+\theta)} \tag{4}$$

The pressure losses in the liquid and vapor phases are expressed as [32]

$$\Delta P_v = F_v L_{eff} Q \tag{5}$$

$$\Delta P_l = F_l L_{eff} Q \tag{6}$$

L_{eff} is the effective length which is defined as L_a + 0.5 (L_e + L_c) where L_a, L_e, and L_c are the lengths of the adiabatic, evaporation, and condensation zones, respectively. F_v and F_l are the friction coefficients in the vapor and liquid phases, and Q is the heat input power.

The axial and radial hydrostatic pressures are calculated as follows [32]

$$\Delta P_{g,axial} = \rho_{nf} g L_t \sin(\psi) \tag{7}$$

$$\Delta P_{g,radial} = \rho_{nf} g D_v \cos(\psi) \tag{8}$$

ρ_{nf} is the nanofluid density. ψ is the tilt angle with respect to the horizontal, and D_v is the vapor diameter. g is the acceleration of gravity.

Referring to Eq. (1), the capillary limit can be expressed as

$$Q_{max} = \frac{(\Delta P_c - \Delta P_{g,radial}) \pm \Delta P_{g,axial}}{(F_l + F_v)\, L_{\text{eff}}} \tag{9}$$

The positive sign in the numerator of Eq. (9) corresponds to the thermosyphon orientation for which the condenser is raised to the evaporator, while the negative sign coincides with the anti-gravity configuration for which the evaporator is mounted above the condenser.

The vapor friction coefficient, F_v, is defined as follows [32]

$$F_v = \frac{\mu_v}{K_v \bar{A}_v \rho_v \Delta h_v} \tag{10}$$

$\bar{A}_v$ is the mean vapor cross-section. ρ_v and μ_v are the vapor density and dynamic viscosity, respectively, and K_v is the permeability for the vapor flow [32]

$$K_v = \frac{D_{hv}^2}{2 P_{ov}} \text{ with } D_{\text{hv}} = \frac{4 \bar{A}_v}{p_v} \tag{11}$$

D_{hv} is the hydraulic diameter of the vapor phase, and Po_v is the Poiseuille number which is equal to 16 since the vapor flow is assumed to be circular. p_v is the perimeter wetted by the vapor phase.

The liquid friction coefficient, F_l, is computed as follows [32]

$$F_l = \frac{\mu_{nf}}{K_g \bar{A}_l \rho_{nf} \Delta h_v} \tag{12}$$

μ_{nf} and ρ_{nf} are the dynamic viscosity and density of the nanofluid, respectively. $\bar{A}_l$ is the mean liquid cross-section, and K_g is the groove permeability which is given by the following relation [32]

$$K_g = \frac{D_{hl}^2 \phi_g}{2 P_{ol}} \text{ with } D_{\text{hl}} = \frac{4 \bar{A}_l}{p_l} \tag{13}$$

D_{hl} corresponds to the hydraulic diameter of the liquid phase, and p_l is the perimeter wetted by the liquid. ϕ_g is the groove porosity which is given by

$$\phi_g = \frac{0.5\ W_{gb} + D_g/tan(\pi/2-\beta)}{W_{gt}} \tag{14}$$

The Poiseuille number for the liquid flow, Po_l, is calculated as follows [33]

if $D_g/W_{gb} \langle 1.5$

$$Po_l = y_o + a \times exp(-b \times \alpha) + c \times \alpha$$

$$\begin{cases} y_o = 6.391\ \theta^{0.1721} \\ a = 137 - 5.008\ \theta + 0.07312\ \theta^2 - 0.0003808\ \theta^3 \\ b = 4.901 + 0.01448\ \theta \\ c = -0.8141 + 0.141\ \theta - 2.762^{-3\theta^2} - 1.758^{-5\theta^3} \end{cases} \tag{15}$$

if $D_g/W_{gb} \rangle 1.5$

$$Po = a \times exp(-0.5 \times (log(\alpha/x_o)/b)^2)$$

$$\begin{cases} a = 11.23\ \theta^{0.09313} \\ b = 2.406\ \theta^{0.01303} \\ x_o = 19.29\ \theta^{-0.3836} \end{cases} \tag{16}$$

The liquid flow areas of the liquid and the vapor phases depend on the meniscus radius of curvature. In Eq. (10), Eq. (11), Eq. (12), and Eq. (13), mean values of A_l and A_v are considered. These values are estimated by integrating the local cross-sectional areas along the FMHP, considering that the curvature radius varies linearly between the value taken in the evaporator zone (r_{ce}) and that taken in the condenser zone (r_{cc}). $\bar{A}_l$ and $\bar{A}_v$ are expressed as (Appendice 1)

$$\bar{A}_l = a_l - b_l\ (r_{ce}^2 + r_{ce}\ r_{cc} + r_{cc}^2) \tag{17}$$

$$\bar{A}_v = a_v + b_v\ (r_{ce}^2 + r_{ce}\ r_{cc} + r_{cc}^2) \tag{18}$$

$$a_l = N_g \left(\left(W_{gb} + D_g\ \tan(\beta) \right)\ D_g \right) \tag{19}$$

$$b_l = b_v = N_g \frac{(\varphi - cos(\varphi)\ sin(\varphi))}{3} \tag{20}$$

$$a_v = \frac{\pi\ D_v^2}{4} \tag{21}$$

$$\varphi = \frac{\pi}{2} - (\beta + \theta) \tag{22}$$

The perimeters p_l and p_v are defined by

$$p_l = N_g \left(\frac{2\ D_g}{\cos(\beta)} + W_{gb} \right) \tag{23}$$

$$p_v = \pi\ D_v \tag{24}$$

4.2 Modeling of the Heat Transfer

The heat transfer mechanisms in a heat pipe are various and the thermal resistance network depicted in Figure 3 can sketch them. Hence, the thermal resistances that are implied in this network are: (1) R_1 and R_7 which correspond to the radial conduction through the evaporator and the condenser walls, (2) R_8 which is due to the axial conduction along the heat pipe wall, (3) R_2 and R_6, which correspond to the evaporation and condensation, (4) R_3 and R_5 due to the heat exchanges by phase change at the liquid-vapor interfaces, and (5) R_4 due to the exchanges by convection between the vapor and the heat pipe wall.

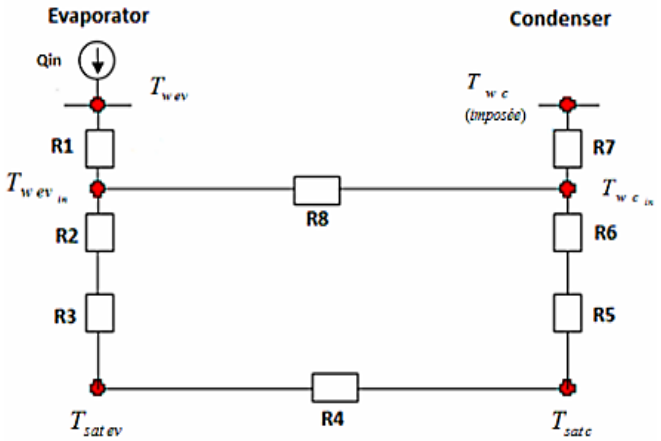

Fig. 3. Thermal resistance network illustrating the heat exchanges in the heat pipe

The heat pipe's overall thermal resistance, R_{tht} is given by

$$R_{tht} = \sum_{i=1}^{7} R_i \tag{25}$$

R_{tht} is calculated by hypothesizing that the thermal resistance R_8 due to the axial conduction along the heat pipe is elevated so that all the heat input power is supposed to be transferred within the heat pipe by phase change.

The thermal resistances R_3 and R_5 are calculated as [32]

$$R_3 = R_5 = \frac{T_{sat}\sqrt{2\pi\, r\, T_{sat}}}{\rho_{\mathrm{nf}}\, \Delta h_v}\frac{(2-\alpha)}{\alpha} \tag{26}$$

α is the accommodation coefficient (generally equal to 1), and r is the gas constant (r = 462 J/kg.K for the vapor). T_{sat} is the saturation temperature, and Δh_v is the latent heat of vaporization.

The thermal resistance R_4 is given by [32]

$$R_4 = \frac{T_{sat}\, \Delta P_v}{\rho_v\, \Delta h_v\, Q} \tag{27}$$

The wall thermal resistance, R_w, is given by

$$R_w = \frac{1}{2\,\pi\,\lambda_{\mathrm{w}}\,\ell}\ln\left(\frac{D_o}{D_i}\right) \tag{28}$$

D_o and D_i are the outer and inner diameters, respectively. λ_w is the wall's thermal conductivity. For the evaporator section, $R_w = R_1$ for which $l = L_e$, and for the condenser section, $R_w = R_7$ for which $l = L_c$.

R_2 and R_6 are determined according to

$$R_2 = \frac{1}{h_v \, \mathrm{A_{ev}}} \tag{29}$$

$$R_6 = \frac{1}{h_c \, \mathrm{A}_c} \tag{30}$$

h_{ev} and h_c are the heat transfer coefficient of evaporation and condensation, respectively. A_{ev} and A_c are the evaporator and condensation heat transfer areas, respectively.

The heat transfer coefficients of evaporation and condensation can be determined by the following correlation [34]

$$Nu = A\, Re^{m_1}\, Pr^{m_2}\, Ja^{*m_3} K_p^{m_4} \tag{31}$$

In Eq. (31), the dimensionless numbers are defined as follows

(i) the Reynolds number

$$Re = \frac{Q}{\mu_{nf}\, \pi\, D_o\, \Delta h_v} \tag{32}$$

where Q is the heat flux rate.

(ii) the Prandtl number

$$Pr = \frac{\mu_{nf}\, c_{p_{nf}}}{\lambda_{nf}} \tag{33}$$

c_{pnf} and λ_{nf} are the specific heat and the thermal conductivity of the nanofluid, respectively.

(iii) the Nusselt number

$$Nu = \frac{h\, L}{\lambda_{nf}} \tag{34}$$

h is the heat transfer coefficient in the evaporator or condenser section, and L is a reference length which is expressed as

For evaporation

$$L_{(ev)} = \sqrt{\frac{\sigma}{(\rho_{nf} - \rho_v) g}} \tag{35}$$

For condensation

$$L_{(c)} = \left(\frac{\nu_{nf}^2}{g}\right)^{1/3} \quad (36)$$

ν_{nf} is the kinematic viscosity of the nanofluid.

(iv) the Jakob number

$$Ja* = \frac{\rho_{nf}}{\rho_v} \frac{c_{p_{nf}} T_{sat}}{\Delta h_v} \quad (37)$$

(v) The Kutateladze number

$$K_p = \frac{P_{sat} L_{(ev)}}{\sigma} \quad (38)$$

P_{sat} is the saturation pressure.

A, m_1, m_2, and m_3 are constants, which are determined from the experimental results. For the evaporation heat transfer, relation (31) is calculated by taking the liquid physical properties at the saturation temperature and the vapor physical properties at the film temperature ($T_f = (T_{sat} + T_w)/2$). For the condensation heat transfer, the liquid and vapor physical properties are determined by considering the film and saturation temperatures, respectively.

The constants of Eq. (31) are obtained from the experimental data by linear regression analysis, for the evaporation and the condensation phenomena [34]. It is found that the heat transfer law proposed by Eq. (31) and the experimental results are well correlated when considering A = 339.3, m_1 = -0.978, m_2 = -0.968, m_3 = 0.205, and m_4 = 1.586, for the evaporation phenomenon, and A = 10.1, m_1 = 0.384, m_2 = - 1.738, m_3 = - 1.099, and m_4 = 0, for the condensation phenomenon. The validity of Eq. (31) is insured for the dimensionless numbers ranging in the intervals which are listed in Table 3.

Table 3
Interval range for the dimensionless numbers in correlation (31) [25]

Evaporation	Condensation
$1 \leq Re \leq 16$	$0.2 \leq Re \leq 3.6$
$2.7 \leq Pr \leq 6.6$	$2.9 \leq Pr \leq 7.5$
$108 \leq K_p \leq 980$	$1.4 \leq K_p \leq 7.5$
$127 \leq Ja^* \leq 11{,}628$	

4.3 Thermophysical Properties of the Nanofluids

In this section, we present the main models adopted in the literature to determine the main thermophysical properties of nanofluids. The models of thermal conductivity, dynamic viscosity, density, and specific heat are highlighted. Although the surface tension and the latent heat of vaporization are important parameters in heat pipe applications, their models are still a debate by the scientific community since the experimental results relative to the determination of these parameters in the case of nanofluids are contradictory.

In all expressions that follow in Table 4, the subscripts “fb” and “np” are referred to as base fluid and nanoparticle, respectively. ϕ_v represents the volume concentration of the nanoparticles.

Table 4
Models of the thermophysical properties of the nanofluid

Physical parameter/Expression		Reference
Thermal conductivity		
$\frac{\lambda_{nf}}{\lambda_{fb}} = \frac{\lambda_{np}+2\lambda_{fb}-2\,c\,(\lambda_{fb}-\lambda_{np})}{\lambda_{np}+2\lambda_{fb}+2\,c\,(\lambda_{fb}-\lambda_{np})}$	(39)	Maxwell [35]
$\phi_v \left(\frac{\lambda_{np}-\lambda_{nf}}{\lambda_{np}+2\lambda_{nf}}\right) + (1 - \phi_v) \left(\frac{\lambda_{fb}-\lambda_{nf}}{\lambda_{fb}+2\lambda_{nf}}\right) = 0$	(40)	Bruggeman [36]
$\frac{\lambda_{nf}}{\lambda_{fb}} = \frac{\lambda_{np} + (n-1)\,\lambda_{fb}-(n-1)\,(\lambda_{fb}-\lambda_{np})\,\phi_v}{\lambda_{np} + (n-1)\,\lambda_{fb}+(n-1)\,(\lambda_{fb}-\lambda_{np})\,\phi_v}$	(41)	Hamilton and Crosser [37]
For spherical particles, $n = 3$ For cylindrical particles, $n = 6$		
Dynamic viscosity		
$\mu_{nf} = \mu_{fb}\,(1 + 2.5\,\phi_v)$	(42)	Einstein [38]
$\mu_{nf} = \mu_{fb} \left(\frac{1}{(1-\phi_v)^{2.5}}\right)$	(43)	Brinkman [39]
$\mu_{nf} = \mu_{fb}\,(1 + \eta\,\phi_v + k_H\,\phi_v^2)$	(44)	Batchelor [40]
k_H is the Huggins coefficient. for spherical particles, $\eta = 2.5$ and $k_H = 6.5$		
$\frac{\mu_{nf}}{\mu_{fb}} = 1 + 2.5\,\phi_v + 4.5 \left[\frac{1}{\left(\frac{h}{d_{np}}\right)\left(2+\frac{h}{d_{np}}\right)\left(1+\frac{h}{d_{np}}\right)^2}\right]$	(45)	Graham [41]
d_{np} and h are the diameter of the particle and the distance between the particles, respectively.		
$\mu_{nf} = \mu_{fb} \left(1 - \frac{\phi_v}{\phi_m}\right)^{-\eta\phi_m}$	(46)	Krieger and Dougherty [42]
Density		
$\rho_{nf} = \phi_v\,\rho_{np} + (1-\phi_v)\,\rho_{fb}$	(47)	Maron and Pierce [43]
Specific heat		
$c_{p,nf} = \phi_v\,c_{p,np} + (1-\phi_v)\,c_{p,fb}$	(48)	Pak and Cho [44]
$(\rho\,c_p)_{nf} = \phi_v\,(\rho\,c_p)_{np} + (1-\phi_v)\,(\rho\,c_p)_{fb}$	(49)	Xuan and Roetzel [45]
Latent heat		
$(\rho\,\Delta h_v)_{nf} = (1-\phi_v)\,(\Delta h_v)_{fb} + \phi_v\,(T_{b,fb}/T_{b,np})\,(\Delta h_v)_{np}$	(50)	Zhou *et al.,* [46]
T_b is the boiling point		
Surface tension		
$\sigma_{nf} = (1-\varphi_v)\,\sigma_{fb}$	(51)	Venkatachalapathy *et al.,* [47]

5. Results and Discussion

In this section, we present the simulated results obtained for two nanofluids: CuO (ρ_{np} = 6450 kg/m^3, c_{pnp} = 561 J/kg.K, λ_{np} = 20 W/m.K) and Al_2O_3 (ρ_{np} = 3960 kg/m^3, cp_{np} = 561.5 J/kg.K, λ_{np} = 37.1 W/m.K) under different nanoparticle concentrations and heat sink temperatures. The main output parameters are the capillary limit, the heat pipe thermal resistance, and the evaporator wall temperature. They are compared to those obtained when the heat pipe is filled with pure water. Besides, the capillary limits reached with water/CuO nanofluid are compared to those obtained with water/Al_2O_3 nanofluid. Since the contact angle affects the results, its value is fixed to 40 ° in these simulations [30].

The variations of the capillary limit, Q_{max}, as a function of the heat sink temperature, T_{hs}, are depicted in Figure 4, for different CuO concentrations (Figure 4(a)) and Al_2O_3 concentrations (Figure

4(b)). For both nanofluids, and a given nanoparticle concentration, the capillary limit increases with the heat sink temperature. Similarly, for a given heat sink temperature, the capillary limit increases with the nanoparticle concentration.

The increase of the capillary limit with the heat sink temperature is due to the reduction of the pressure losses in the liquid and vapor phases caused by the decrease of the dynamic viscosity with temperature. It should be noted that the driving capillary pressure also decreases with the heat sink temperature due to the reduction of the surface tension with the temperature. However, this decrease is less significant than that of the pressure drops in the liquid and vapor phases. Consequently, the maximum heat transport capacity of the heat pipe is enhanced.

As the nanoparticle concentration increases, the density and the dynamic viscosity increase. The liquid friction coefficient, F_l, which is expressed by (Eq. (12)), decreases because the increase in density is greater than that of the dynamic viscosity, and the latent heat is hardly affected by the nanoparticle concentration. Thus, the pressure losses in the liquid phase, which are more preponderant than those in the vapor phase, decrease. The vapor pressure losses are not affected by the nanoparticle concentration since the vapor friction coefficient, F_v, depends mainly on the vapor thermophysical properties. Thus, the overall pressure losses decrease, and consequently, the capillary limit increases.

The variations of the increase in the capillary limit obtained with the water/CuO nanofluid with respect to that obtained with pure water are presented in Figure 5(a). For a heat sink temperature, T_{hs} = 25 °C, the capillary limit improvement varies between 4 % for ϕ_v = 1 % and 20 % for ϕ_v = 5 %, whereas it varies from 5 % to 25 % for T_{hs} = 55 °C. For water/Al_2O_3 nanofluid, the capillary improvement is lower (Figure 5(b)). Indeed, for T_{hs} = 25 °C, it varies from 2.4 % to 11.8 % when ϕ_v increases from 1 % to 5 %, whereas for T_{hs} = 55 °C, it varies from 2.7 % to 13.8 % for the same concentration range. Figure 6 compares the values of Q_{max} obtained with water/CuO nanofluid and those obtained with water/Al_2O_3 nanofluid for different nanoparticle concentrations and heat sink temperatures. For a given heat sink temperature, T_{hs}, the capillary limit obtained with water/CuO nanofluid is higher than that obtained with water/Al_2O_3 nanofluid, and the relative gap increases with the concentration and heat sink temperature. Thus, for T_{hs} = 25 °C, the relative gap varies from 1.5 % to 7.1 % when ϕ_v increases from 1 % to 5 %, while for T_{hs} = 55 °C, the relative gap increases from 2.1 % to 8.8 % when ϕ_v increases from 1 % to 5 %. The water/CuO nanofluid allows for better performance than water/Al_2O_3 because the thermophysical properties (density and dynamic viscosity) of CuO allow for a lower liquid friction coefficient.

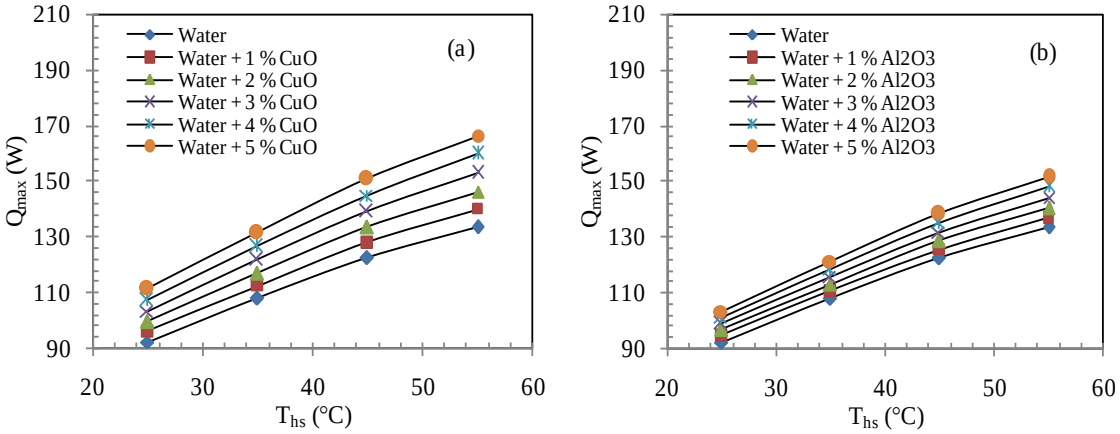

Fig. 4. Variations of the capillary limit with T_{hs}, for different nanoparticle concentrations: (a) water/CuO, (b) water/Al_2O_3

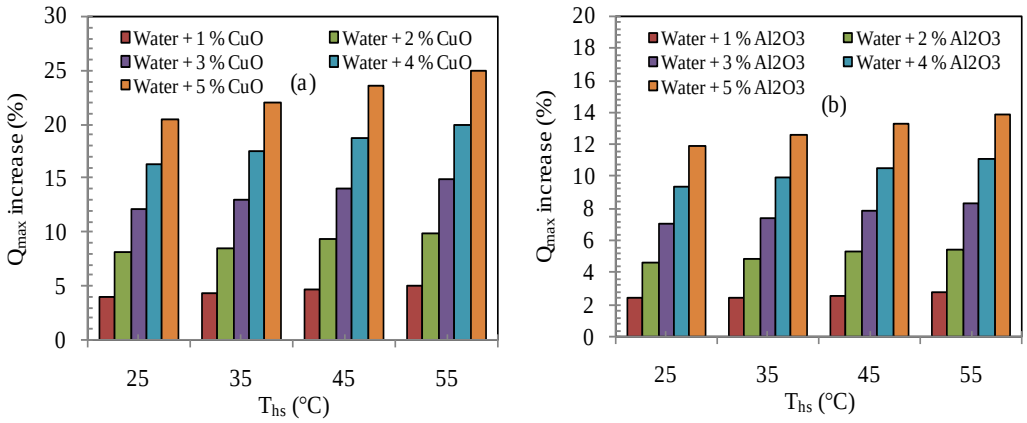

Fig. 5. Comparison between the capillary limit obtained with the nanofluid and that obtained with pure water: (a) water/CuO, (b) water/Al_2O_3

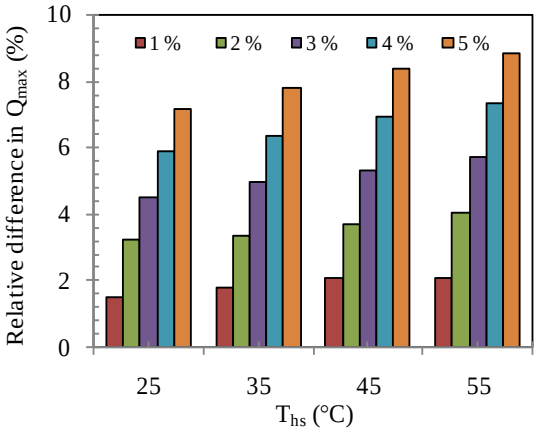

Fig. 6. Comparison between the capillary limit obtained with water/CuO and that obtained with water/Al_2O_3

Figure 7 depicts the variations of the heat pipe thermal resistance, R_{tht}, as a function of the heat sink temperature, T_{hs}, for water/CuO nanofluid (Figure 7(a)) and water/Al_2O_3 nanofluid (Figure 7(b)), for different nanoparticle concentrations. For a given nanoparticle concentration, the thermal resistance decreases with the heat sink temperature. Similarly, for a given heat sink temperature, T_{hs}, the thermal resistance decreases with the nanoparticle concentration. For a given temperature, T_{hs}, the reduction in the heat pipe thermal resistance obtained with the nanofluid increases with the nanoparticle concentration (Figure 8). Thus, for the water/CuO nanofluid, and T_{hs} = 25 °C, the reduction in the heat pipe thermal resistance increases from 24.6 % to 64.8 % when the nanoparticle concentration increases from 1 to 5 % (Figure 8(a)). For the water/Al_2O_3 nanofluid, this reduction is smaller and increases from 16.1 % to 48.7 % under the same conditions (Figure 8(b)). Moreover, it should be noted that for a given nanoparticle concentration, this reduction is hardly affected by the heat sink temperature for both nanofluids. For T_{hs} = 55 ° C, and the water/CuO nanofluid, it varies from 26.9 % to 67.9 % when ϕ_v increases from 1 % to 5 %, whereas for the water/Al_2O_3 nanofluid, it varies from 17.2 % to 50.7 % under the same conditions. The variations of the relative difference between the heat pipe thermal resistance obtained with the water/CuO nanofluid and that obtained with the water/Al_2O_3 nanofluid are depicted in Figure 9. The heat pipe thermal resistance obtained with water/CuO nanofluid is lower than that obtained with water/Al_2O_3 nanofluid. The relative difference values that are plotted in Figure 9 are absolute. For T_{hs} = 25 °C, the relative difference

increases from 11.3 % to 45.7 % when the nanoparticle concentration increases from 1 % to 5 %. This relative difference also increases with the heat sink temperature, T_{hs}. Indeed, for T_{hs} = 55 °C, it varies from 13.3 % to 53.5 % when the nanoparticle concentration increases from 1 % to 5 %. The low thermal resistances obtained with water/CuO nanofluid are mainly attributed to the high heat transfer coefficient of evaporation and condensation obtained with this nanofluid.

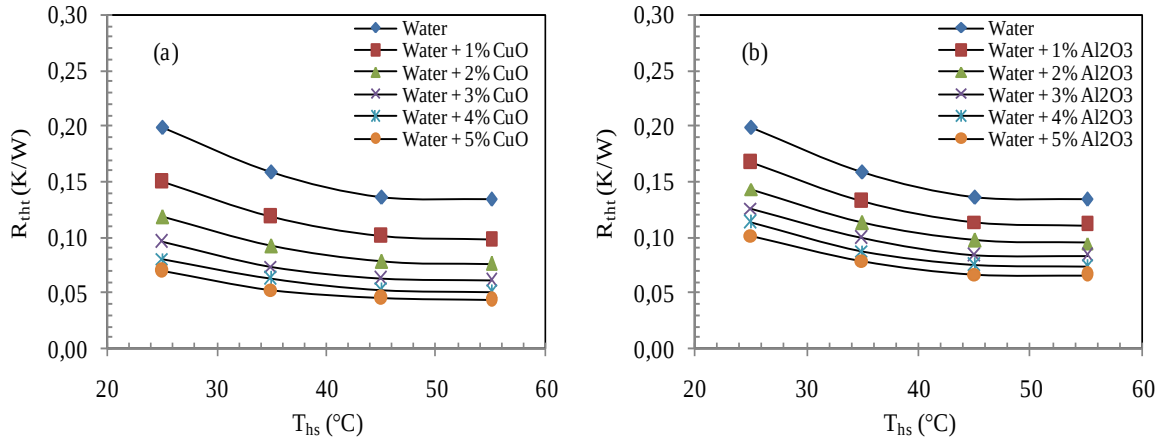

Fig. 7. Variations of the heat pipe thermal resistance with T_{hs}, for different nanoparticle concentrations: (a) water/CuO, (b) water/Al_2O_3

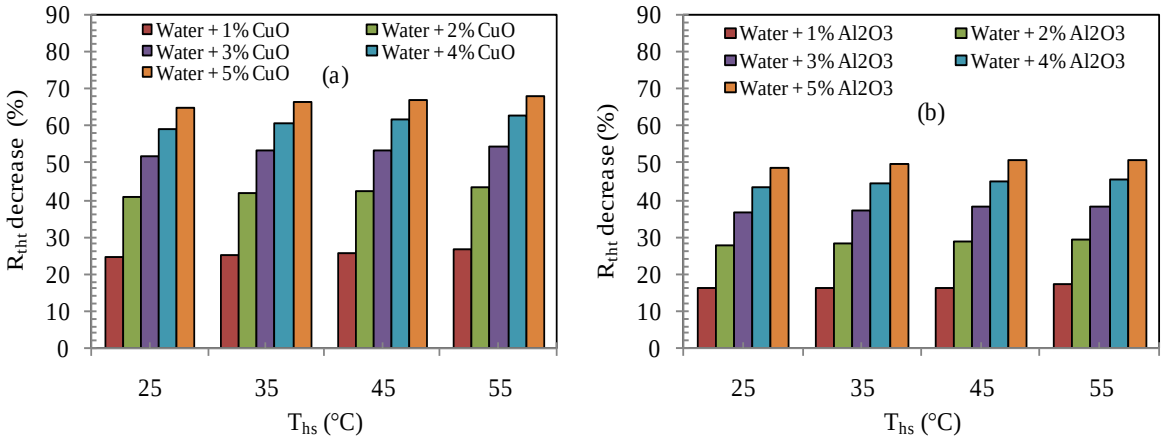

Fig. 8. Comparison between the heat pipe thermal resistance obtained with the nanofluid and that obtained with pure water: (a) water/CuO, (b) water/Al_2O_3

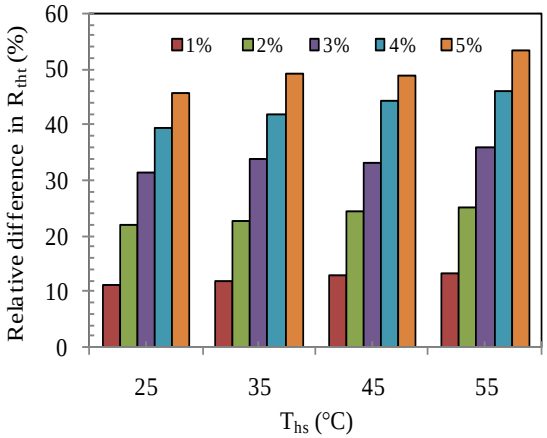

Fig. 9. Comparison between the thermal resistance obtained with water/CuO and that obtained with water/Al_2O_3

The variations of the evaporator wall temperature, T_{wev}, as a function of T_{hs}, for different nanoparticle concentrations, ϕ_v, for the two nanofluids, are shown in Figure 10. For a given nanoparticle concentration, the evaporator wall temperature rises with the heat sink temperature. Nevertheless, for a given heat sink temperature, the temperature of the evaporator wall decreases when the nanoparticles are added. The variations in the reduction of the evaporator wall temperature obtained with a nanofluid when compared to that obtained with pure water are shown in Figure 11. For a given heat sink temperature, T_{hs}, this reduction increases with the nanoparticle concentration; however, for a given nanoparticle concentration, it decreases with T_{hs}. Thus, with a 1 % concentration of CuO nanoparticles, and for T_{hs} = 25 °C, the reduction in the wall temperature of the evaporator is 9.3 %; whereas this reduction is 5.5 % for T_{hs} = 55 °C (Figure 11(a)). A CuO nanoparticle concentration of 5 % allows us to obtain relative reductions of 24.3 % and 14.6 % for T_{hs} = 25 °C and 55 °C, respectively (Figure 11(a)). For 1 % concentration for Al_2O_3 nanoparticles, the evaporator wall temperature reduction is 5.8 % for T_{hs} = 25 °C and 3.6 % for T_{hs} = 55 °C (Figure 11(b)). For a concentration of 5 %, the decrease in the evaporator wall temperature is more significant. It is 18.1 % for T_{hs} = 25 °C and 10.7 % for T_{hs} = 55 °C (Figure 11(b)). The variations of the relative difference between the evaporator wall temperature obtained with the water/CuO nanofluid and that obtained with water/Al_2O_3 nanofluid are shown in Figure 12. The values reported in this figure are absolute since the evaporator wall temperatures obtained with CuO nanoparticles are lower than those reached with Al_2O_3 nanoparticles. For a given, T_{hs}, this difference increases with the nanoparticle concentration. For a given nanoparticle concentration, the variations of this relative difference are not monotonous. Indeed, for nanoparticle concentrations less than 2 %, the relative difference diminishes as the heat sink temperature increases. For nanoparticle concentrations greater than 2 %, this relative difference exhibits a minimum indicating the existence of an optimum heat sink temperature allowing to obtain a minimum evaporator wall temperature.

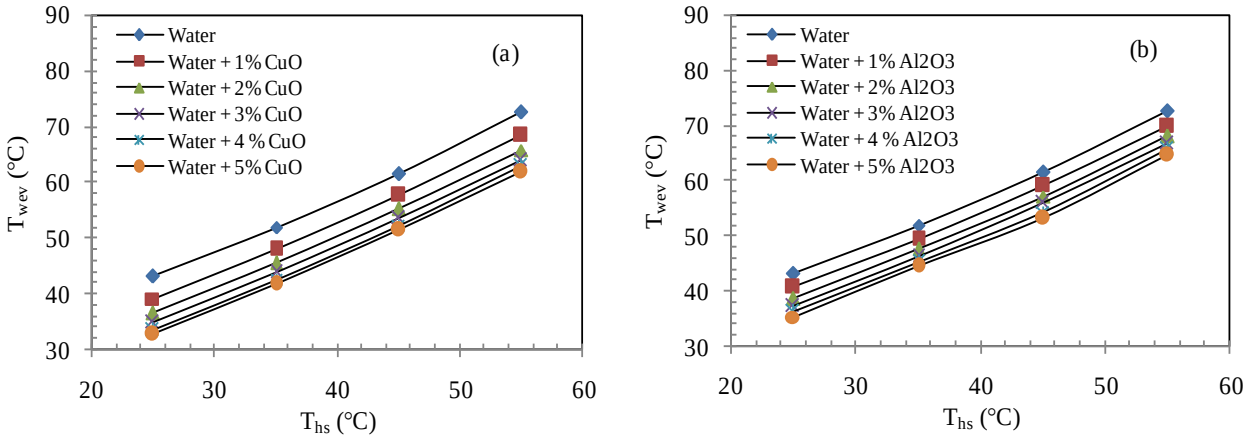

Fig. 10. Evolution of the evaporator wall temperature with T_{hs}, for different nanoparticle concentrations: (a) water/CuO, (b) water/Al_2O_3

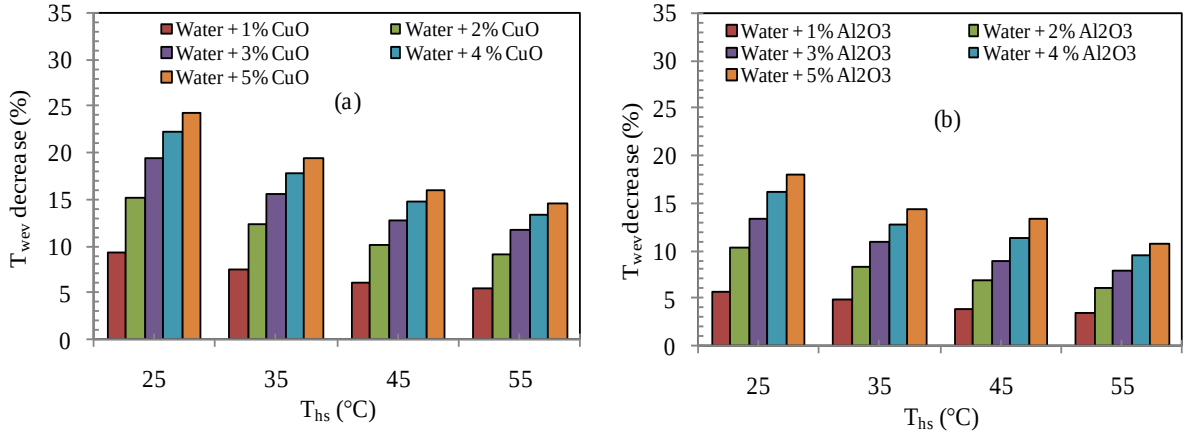

Fig. 11. Comparison between the evaporator wall temperature obtained with the nanofluid and that obtained with pure water: (a) water/CuO, (b) water/Al_2O_3

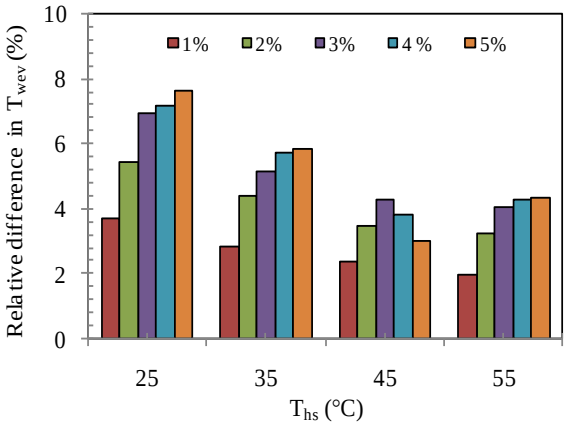

Fig. 12. Comparison between the evaporator wall temperature obtained with water/CuO and that obtained with water/Al_2O_3

6. Conclusions

A mathematical model is presented to study the capillary limit and the heat transfer performances of a nanofluid-filled cylindrical copper heat pipe including a capillary structure composed of helicoidal and trapezoidal grooves. Two nanofluids are considered: water/CuO and water/Al_2O_3.

The capillary limit is determined by analyzing the liquid and vapor pressure drops along the heat pipe. The friction factors, which are considered in the pressure drop analysis, are a function of the Poiseuille numbers that are calculated from expressions issued from the analytical model of Kim *et al.,* [33]. The capillary radii in the evaporator and condenser regions are determined based on geometrical considerations.

The heat transfer analysis is determined by considering the different thermal resistances. The evaporator and condenser thermal resistances are the highest ones and they are calculated from correlations determined from experiments with the same dimensions and including the same capillary grooves as those for the modeled heat pipe. These correlations include dimensionless numbers of which the values ranges are still valid for the studied nanofluids in different operating conditions.

The results indicate that compared to the water-filled heat pipe, the nanofluid-filled heat pipe allows for up to 25 % and 14 % increase in the capillary limit for water/CuO and water/Al_2O_3 nanofluids, respectively. Also, reductions up to 68 % and up to 51 % in the heat pipe thermal resistances are obtained for water/CuO and water/Al_2O_3 nanofluids, respectively. Moreover, decreases up to 24 %, and up to 18 % in the evaporator wall temperatures are obtained for water/CuO and water/Al_2O_3 nanofluids, respectively. Besides, the thermal performances obtained with water/CuO nanofluid are higher than those obtained with water/Al_2O_3 nanofluid.

More research is needed to design, develop, and optimize the thermal performance of the nanofluid-filled heat pipes.

i. More theoretical studies must be carried out to optimize the input parameters such as heat input power, tilt angle, fill charge, nanoparticle concentration, and size of nanoparticles.
ii. The use of hybrid nanofluids in heat pipes is in the early stage. Therefore, more theoretical studies should be conducted in future research to simulate the heat pipe thermal performance filled with hybrid nanofluids.
iii. Predictive methods based on machine learning methods like artificial neural networks (ANNs), can be used to provide reliable and strong predictions of the nanofluid-filled heat pipe.

References

[1] Driss, Améni, Samah Maalej, and Mohamed Chaker Zaghdoudi. "Experimentation and modeling of the steady-state and transient thermal performances of a helicoidally grooved cylindrical heat pipe." *Microelectronics Reliability* 62 (2016): 102-112. https://doi.org/10.1016/j.microrel.2016.03.022

[2] Driss, A., M. B. H. Sassi, S. Maalej, and M. C. Zaghdoudi. "Transient thermal performance modeling and experimentation of heat pipes for high power electronics cooling." *International Review on Modeling and Simulations (IREMOS)* 5, no. 6 (2012): 2473-2483.

[3] Driss, Améni, Samah Maalej, and Mohamed Chaker Zaghdoudi. "Electro-Thermal Modeling of Power IGBT Module Cooled by A Heat Pipe Cooling System." *Journal of Advanced Research in Fluid Mechanics and Thermal Sciences* 86, no. 1 (2021): 105-122. https://doi.org/10.37934/arfmts.86.1.105122

[4] Saad, I., S. Maalej, and M. C. Zaghdoudi. "Numerical study of the electrohydrodynamic effects on the two-phase flow within an axially grooved flat miniature heat pipe." *International Journal of Heat and Mass Transfer* 107 (2017): 244-263. https://doi.org/10.1016/j.ijheatmasstransfer.2016.10.089

[5] Saad, I., S. Maalej, and M. C. Zaghdoudi. "Combined effects of heat input power and filling fluid charge on the thermal performance of an electrohydrodynamic axially grooved flat miniature heat pipe." *Applied Thermal Engineering* 134 (2018): 469-483. https://doi.org/10.1016/j.applthermaleng.2018.01.099

[6] Saad, Imène, Samah Maalej, and Mohamed Chaker Zaghdoudi. "Numerical investigation on the dielectric working fluid effect on the flow and thermal parameters of an electrohydrodynamic flat heat pipe." *Journal of Advanced Research in Fluid Mechanics and Thermal Sciences* 79, no. 1 (2020): 128-152. https://doi.org/10.37934/arfmts.79.1.128152

[7] Park, Ki-Ho, Wook-Hyun Lee, K. W. Lee, I. H. Baek, S. H. Rhi, and Dong-Reun Shin. "Study on the operating characteristics in small size heat pipe using nanofluids." In *Proceedings of the 3rd IASME/WSEAS International Conference on Heat Transfer, Thermal Engineering and Environment*: August 20-22, 2005; Corfu, Greece, pp. 106-109. 2005. Environment, Greece, pp. 20-22, 2005.

[8] Wei, Wei-Chiang, Sheng-Hong Tsai, Shih-Yu Yang, and Shung-Wen Kang. "Effect of nanofluid concentration on heat pipe thermal performance." *IASME Trans* 2, no. 8 (2005): 1432-1439.

[9] Kang, Shung-Wen, Wei-Chiang Wei, Sheng-Hong Tsai, and Shih-Yu Yang. "Experimental investigation of silver nano-fluid on heat pipe thermal performance." *Applied Thermal Engineering* 26, no. 17-18 (2006): 2377-2382. https://doi.org/10.1016/j.applthermaleng.2006.02.020

[10] Naphon, Paisarn, Pichai Assadamongkol, and Teerapong Borirak. "Experimental investigation of titanium nanofluids on the heat pipe thermal efficiency." *International Communications in Heat and Mass Transfer* 35, no. 10 (2008): 1316-1319. https://doi.org/10.1016/j.icheatmasstransfer.2008.07.010

[11] Yang, Xue Fei, Zhen-Hua Liu, and Jie Zhao. "Heat transfer performance of a horizontal micro-grooved heat pipe using CuO nanofluid." *Journal of Micromechanics and Microengineering* 18, no. 3 (2008): 035038. https://doi.org/10.1088/0960-1317/18/3/035038

[12] Liu, Zhen-Hua, and Lin Lu. "Thermal performance of axially microgrooved heat pipe using carbon nanotube suspensions." *Journal of Thermophysics and Heat Transfer* 23, no. 1 (2009): 170-175. https://doi.org/10.2514/1.38190

[13] Naphon, Paisarn, Dithapong Thongkum, and Pichai Assadamongkol. "Heat pipe efficiency enhancement with refrigerant-nanoparticles mixtures." *Energy Conversion and Management* 50, no. 3 (2009): 772-776. https://doi.org/10.1016/j.enconman.2008.09.045

[14] Liu, Zhen-Hua, Yuan-Yang Li, and Ran Bao. "Thermal performance of inclined grooved heat pipes using nanofluids." *International Journal of Thermal Sciences* 49, no. 9 (2010): 1680-1687. https://doi.org/10.1016/j.ijthermalsci.2010.03.006

[15] Teng, Tun-Ping, How-Gao Hsu, Huai-En Mo, and Chien-Chih Chen. "Thermal efficiency of heat pipe with alumina nanofluid." *Journal of Alloys and Compounds* 504 (2010): S380-S384. https://doi.org/10.1016/j.jallcom.2010.02.046

[16] Wang, Guo-Shan, Bin Song, and Zhen-Hua Liu. "Operation characteristics of cylindrical miniature grooved heat pipe using aqueous CuO nanofluids." *Experimental Thermal and Fluid Science* 34, no. 8 (2010): 1415-1421. https://doi.org/10.1016/j.expthermflusci.2010.07.004

[17] Han, Woo-Sung, and Seok-Ho Rhi. "Thermal characteristics of grooved heat pipe with hybrid nanofluids." *Thermal Science* 15, no. 1 (2011): 195-206. https://doi.org/10.2298/TSCI100209056H

[18] Liu, Zhen-Hua, Yuan-Yang Li, and Ran Bao. "Compositive effect of nanoparticle parameter on thermal performance of cylindrical micro-grooved heat pipe using nanofluids." *International Journal of Thermal Sciences* 50, no. 4 (2011): 558-568. https://doi.org/10.1016/j.ijthermalsci.2010.11.013

[19] Ghanbarpour, Morteza, and Rahmatollah Khodabandeh. "Entropy generation analysis of cylindrical heat pipe using nanofluid." *Thermochimica Acta* 610 (2015): 37-46. https://doi.org/10.1016/j.tca.2015.04.028

[20] Yousefi, Tooraj, and Mehdi Heidari. "Thermal performance enhancement of L-shaped microgrooved heat pipe containing water-based Al_2O_3 nanofluids." *Heat Transfer Engineering* 36, no. 5 (2015): 462-470. https://doi.org/10.1080/01457632.2014.935217

[21] Aly, Wael IA, Moustafa A. Elbalshouny, H. M. Abd El-Hameed, and M. Fatouh. "Thermal performance evaluation of a helically-micro-grooved heat pipe working with water and aqueous Al_2O_3 nanofluid at different inclination angle and filling ratio." *Applied Thermal Engineering* 110 (2017): 1294-1304. https://doi.org/10.1016/j.applthermaleng.2016.08.130

[22] Mehrali, Mohammad, Emad Sadeghinezhad, Reza Azizian, Amir Reza Akhiani, Sara Tahan Latibari, Mehdi Mehrali, and Hendrik Simon Cornelis Metselaar. "Effect of nitrogen-doped graphene nanofluid on the thermal performance of the grooved copper heat pipe." *Energy Conversion and Management* 118 (2016): 459-473. https://doi.org/10.1016/j.enconman.2016.04.028

[23] Thosre, Sagar S., Nitin V. Sali, Omkar C. Nikam, and Swaroopsinh B. Bore. "Thermal Performance Investigation of Grooved Tube with Twisted Tape Insert and Al_2O_3 Nanofluid." *International Research Journal of Engineering and Technology (IRJET)* 5, no. 7 (2018): 681-686.
[24] Zhao, Shanguo, Guoying Xu, Ning Wang, and Xiaosong Zhang. "Experimental study on the thermal start-up performance of the graphene/water nanofluid-enhanced solar gravity heat pipe." *Nanomaterials* 8, no. 2 (2018): 72. https://doi.org/10.3390/nano8020072
[25] Gupta, Naveen Kumar, Aman Barua, Shashwat Mishra, Shubham Kumar Singh, Arun Kr Tiwari, and Subrata Kr Ghosh. "Numerical study of CeO_2/H_2O nanofluid application on thermal performance of heat pipe." *Materials Today: Proceedings* 18 (2019): 1006-1016. https://doi.org/10.1016/j.matpr.2019.06.541
[26] Sözen, Adnan, Metin Gürü, Ataollah Khanlari, and Erdem Çiftçi. "Experimental and numerical study on enhancement of heat transfer characteristics of a heat pipe utilizing aqueous clinoptilolite nanofluid." *Applied Thermal Engineering* 160 (2019): 114001. https://doi.org/10.1016/j.applthermaleng.2019.114001
[27] Zhou, Rui, Shengjuan Fu, Hui Li, Dong Yuan, Biao Tang, and Guofu Zhou. "Experimental study on thermal performance of copper nanofluids in a miniature heat pipe fabricated by wire electrical discharge machining." *Applied Thermal Engineering* 160 (2019): 113989. https://doi.org/10.1016/j.applthermaleng.2019.113989
[28] Aydin, Duygu Yilmaz, Metin Gürü, Adnan Sözen, and Erdem Çiftçi. "Thermal performance improvement of the heat pipe by employing dolomite/ethylene glycol nanofluid." *International Journal of Renewable Energy Development* 9, no. 1 (2020): 23. https://doi.org/10.14710/ijred.9.1.23-27
[29] Martin, Kerim, Adnan Sözen, Erdem Çiftçi, and Hafiz Muhammad Ali. "An experimental investigation on aqueous Fe-CuO hybrid nanofluid usage in a plain heat pipe." *International Journal of Thermophysics* 41, no. 9 (2020): 1-21. https://doi.org/10.1007/s10765-020-02716-6
[30] Pandya, Naimish S., Akshaykumar N. Desai, Arun Kumar Tiwari, and Zafar Said. "Influence of the geometrical parameters and particle concentration levels of hybrid nanofluid on the thermal performance of axial grooved heat pipe." *Thermal Science and Engineering Progress* 21 (2021): 100762. https://doi.org/10.1016/j.tsep.2020.100762
[31] Veerasamy, Aruna, Kanimozhi Balakrishnan, Teja Yernagu Surya, and Zaheer Abbas. "Efficiency improvement of heat pipe by using Graphene nanofluids with different concentrations." *Thermal Science* 24, no. 1 Part B (2020): 447-452. https://doi.org/10.2298/TSCI190415358V
[32] Maalej, Samah, Mansouri Jed, and M. C. Zaghdoudi. "Experimental and theoretical analysis on enhanced flat miniature heat pipes with axial capillary grooves and screen meshes." *International Review of Mechanical Engineering* 5, no. 1 (2011): 180-195.
[33] Kim, Sung Jin, Joung Ki Seo, and Kyu Hyung Do. "Analytical and experimental investigation on the operational characteristics and the thermal optimization of a miniature heat pipe with a grooved wick structure." *International Journal of Heat and Mass Transfer* 46, no. 11 (2003): 2051-2063. https://doi.org/10.1016/S0017-9310(02)00504-5
[34] Driss, A., S. Maalej, I. Chouat, and M. C. Zaghdoudi. "Experimental investigation on the thermal performance of a heat pipe-based cooling system." *Mathematical Modeling of Engineering Problems* 6, no. 2 (2019): 217-228. https://doi.org/10.18280/mmep.060209
[35] Maxwell, James Clerk. *A Treatise on Electricity and Magnetism*. Clarendon Press, 1881.
[36] Bruggeman, G. "Calculation of various physics constants in heterogenous substances I Dielectricity Constants and Conductivity of Mixed Bodies from Isotropic Substances." *Annalen der Physik* 416, no. 7 (1935): 636-664. https://doi.org/10.1002/andp.19354160705
[37] Hamilton, R. L., and O. K. Crosser. "Thermal conductivity of heterogeneous two-component systems." *Industrial & Engineering Chemistry Fundamentals* 1, no. 3 (1962): 187-191. https://doi.org/10.1021/i160003a005
[38] Einstein, A. "Eineneuebestimmung der moleküldimensionen." *Annalen der Physik* 19 (1906): 289-306. https://doi.org/10.1002/andp.19063240204
[39] Brinkman, Hendrik C. "The viscosity of concentrated suspensions and solutions." *The Journal of Chemical Physics* 20, no. 4 (1952): 571-581. https://doi.org/10.1063/1.1700493
[40] Batchelor, G. K. "The effect of Brownian motion on the bulk stress in a suspension of spherical particles." *Journal of Fluid Mechanics* 83, no. 1 (1977): 97-117. https://doi.org/10.1017/S0022112077001062
[41] Graham, Alan L. "On the viscosity of suspensions of solid spheres." *Applied Scientific Research* 37, no. 3 (1981): 275-286. https://doi.org/10.1007/BF00951252
[42] Krieger, Irvin M., and Thomas J. Dougherty. "Concentration dependence of the viscosity of suspensions." *Transactions of the Society of Rheology* 3, no. 1 (1959): 137-152. https://doi.org/10.1122/1.548848
[43] Maron, Samuel H., and Percy E. Pierce. "Application of Ree-Eyring generalized flow theory to suspensions of spherical particles." *Journal of Colloid Science* 11, no. 1 (1956): 80-95. https://doi.org/10.1016/0095-8522(56)90023-X

[44] Pak, Bock Choon, and Young I. Cho. "Hydrodynamic and heat transfer study of dispersed fluids with submicron metallic oxide particles." *Experimental Heat Transfer an International Journal* 11, no. 2 (1998): 151-170. https://doi.org/10.1080/08916159808946559

[45] Xuan, Yimin, and Wilfried Roetzel. "Conceptions for heat transfer correlation of nanofluids." *International Journal of Heat and Mass Transfer* 43, no. 19 (2000): 3701-3707. https://doi.org/10.1016/S0017-9310(99)00369-5

[46] Zhou, Le-Ping, Bu-Xuan Wang, Xiao-Feng Peng, Xiao-Ze Du, and Yong-Ping Yang. "On the specific heat capacity of CuO nanofluid." *Advances in Mechanical Engineering* 2 (2010): 172085. https://doi.org/10.1155/2010/172085

[47] Venkatachalapathy, S., G. Kumaresan, and S. Suresh. "Performance analysis of cylindrical heat pipe using nanofluids-An experimental study." *International Journal of Multiphase Flow* 72 (2015): 188-197. https://doi.org/10.1016/j.ijmultiphaseflow.2015.02.006